# *ODC1* Is a Critical Determinant of *MYCN* Oncogenesis and a Therapeutic Target in Neuroblastoma

Michael D. Hogarty,[1,2] Murray D. Norris,[5] Kimberly Davis,[1] Xueyuan Liu,[1] Nicholas F. Evageliou,[1] Candace S. Hayes,[7] Bruce Pawel,[3] Rong Guo,[4] Huaqing Zhao,[4] Eric Sekyere,[5] Joanna Keating,[5] Wayne Thomas,[5] Ngan Ching Cheng,[5] Jayne Murray,[5] Janice Smith,[5] Rosemary Sutton,[5] Nicola Venn,[5] Wendy B. London,[8] Allen Buxton,[8] Susan K. Gilmour,[7] Glenn M. Marshall,[5,6] and Michelle Haber[5]

[1]Division of Oncology, The Children's Hospital of Philadelphia; Departments of [2]Pediatrics, [3]Pathology, and [4]Biostatistics and Epidemiology, University of Pennsylvania School of Medicine, Philadelphia, Pennsylvania; [5]Children's Cancer Institute Australia for Medical Research; [6]Centre for Children's Cancer and Blood Disorders, Sydney Children's Hospital, Randwick, New South Wales, Australia; [7]Lankenau Institute for Medical Research, Wynnewood, Pennsylvania; and [8]Department of Statistics, University of Florida and Children's Oncology Group Statistics and Data Center Department, Gainesville, Florida



## Abstract

**Neuroblastoma is a frequently lethal childhood tumor in which *MYC* gene deregulation, commonly as *MYCN* amplification, portends poor outcome. Identifying the requisite biopathways downstream of *MYC* may provide therapeutic opportunities. We used transcriptome analyses to show that *MYCN*-amplified neuroblastomas have coordinately deregulated myriad polyamine enzymes (including *ODC1, SRM, SMS, AMD1, OAZ2*, and *SMOX*) to enhance polyamine biosynthesis. High-risk tumors without *MYCN* amplification also overexpress *ODC1*, the rate-limiting enzyme in polyamine biosynthesis, when compared with lower-risk tumors, suggesting that this pathway may be pivotal. Indeed, elevated *ODC1* (independent of *MYCN* amplification) was associated with reduced survival in a large independent neuroblastoma cohort. As polyamines are essential for cell survival and linked to cancer progression, we studied polyamine antagonism to test for metabolic dependence on this pathway in neuroblastoma. The Odc inhibitor α-difluoromethylornithine (DFMO) inhibited neuroblast proliferation *in vitro* and suppressed oncogenesis *in vivo*. DFMO treatment of neuroblastoma-prone genetically engineered mice (*TH-MYCN*) extended tumor latency and survival in homozygous mice and prevented oncogenesis in hemizygous mice. In the latter, transient Odc ablation permanently prevented tumor onset consistent with a time-limited window for embryonal tumor initiation. Importantly, we show that DFMO augments antitumor efficacy of conventional cytotoxics *in vivo*. This work implicates polyamine biosynthesis as an arbiter of *MYCN* oncogenesis and shows initial efficacy for polyamine depletion strategies in neuroblastoma, a strategy that may have utility for this and other *MYC*-driven embryonal tumors.** [Cancer Res 2008;68(23):9735–45]

## Introduction

Neuroblastoma is a common childhood tumor arising within the peripheral nervous system. The genetic feature most consistently associated with treatment failure is amplification of the *MYCN* proto-oncogene that strongly correlates with advanced disease (1, 2). Even in otherwise favorable localized disease, *MYCN* amplification portends poor outcome, underscoring its biological importance (3). In high-risk neuroblastomas that lack *MYCN* amplification, *MYC* itself may be deregulated (4, 5). Myc genes (including *MYCN, MYC*, and *MYCL1*) represent a family of basic helix-loop-helix leucine zipper transcription factors that are among the most frequently deregulated genes in cancer. Myc proteins form heterodimers with Max and are recruited to CACGTG (E-box) recognition sequences to transactivate target genes, or enter additional complexes to form repressors (reviewed in refs. 6, 7). It has been estimated that nearly one tenth of all genes may be directly or indirectly regulated by the Myc:Max axis (8), yet the determination of those necessary or sufficient to confer oncogenic properties remains empiric.

One compelling target that may be decisive in mediating *MYC* effects is *ODC1* (9), a bona fide oncogene that encodes the rate-limiting enzyme in polyamine synthesis (10). Polyamines are organic cations that enhance transcription, translation, and replication (11) and support many cellular processes governed by *MYC* genes. Their maintenance is essential for cell survival as depletion activates growth arrest or apoptotic checkpoints (12). Thus, intracellular polyamines are kept under tight control through posttranscriptional as well as transcriptional regulation, with the rate-limiting enzymes *ODC1* and *AMD1* having among the shortest half-lives of any mammalian enzyme as a result (13). Odc activity is frequently elevated in cancer through deregulation of *MYC*, resulting in higher polyamine content to support rapid tumor cell proliferation (11). Considerable evidence links elevated polyamines to colon, breast, prostate, and skin carcinoma progression (14) but not embryonal tumors to date. Recently, the contribution of Odc activity to *MYC*-induced lymphomagenesis was investigated using the Eμ-*MYC* murine model in which transient biochemical ablation inhibited lymphomagenesis, whereas restoration of Odc activity allowed for delayed tumor onset (15).

We therefore sought to define whether Odc-mediated polyamine biosynthesis was a requisite metabolic biopathway supporting embryonal tumor initiation or progression. Most children with high-risk neuroblastoma have tumors that manifest a lethal course despite intensive multimodal therapy (16, 17). Thus, elucidating novel therapeutic pathways is paramount. We show that polyamine expansion through broad deregulation of regulatory enzymes, including *ODC1*, is a hallmark of neuroblastomas with *MYCN*

**Note:** Supplementary data for this article are available at Cancer Research Online (http://cancerres.aacrjournals.org/).

**Requests for reprints:** Michael D. Hogarty, Division of Oncology, The Children's Hospital of Philadelphia, 9 North ARC, Suite 902C, 3615 Civic Center Boulevard, Philadelphia, PA 19104-4318. Phone: 215-590-3931; Fax: 215-590-3770; E-mail: hogartym@email.chop.edu.



doi:10.1158/0008-5472.CAN-07-6866

amplification. High *ODC1* correlates with poor clinical outcome in a large cohort of patients, including those lacking *MYCN* amplification. Further, we show that biochemically disabling Odc inhibits neuroblastoma proliferation *in vitro* and has marked antitumor efficacy in a neuroblastoma-prone transgenic mouse model. Together, these data support that the adequate provision of polyamines is critical for *MYC*-driven proliferation and that targeted disruption of this pathway has therapeutic utility.

## Materials and Methods

### Patient Samples, Expression Profiling, Array Comparative Genomic Hybridization, and Real-time Quantitative PCR

Transcriptome profiles from 101 primary neuroblastomas from Children's Oncology Group (COG) and the Children's Hospital of Philadelphia were obtained by our groups previously. Clinical and genetic features have been reported (18). Briefly, risk class was defined using COG criteria: 28 were localized biologically favorable neuroblastoma (low risk), 21 were intermediate-risk tumors, and 52 were high-risk tumors (of which 20 had *MYCN* amplification). cRNA was hybridized to Affymetrix U95Av2 oligonucleotide arrays containing 12,625 probe sets (Affymetrix) and statistical modeling of probe set behavior was conducted using Probe Profiler (Corimbia). A quantitative expression score (*e*-score) was calculated for each probe set. The data from this experiment are available online.[9] Differential gene expression was measured with the Patterns from Gene Expression (PaGE; ref. 19) algorithm using binary comparisons of *e*-scores. All runs were done with 2001 permutations on unlogged data. A confidence level of 0.95 (1-FDR) was used to define differential expression for these analyses.

A subset of tumors ($n$ = 80) had DNA available for detection of copy number alterations (CNA) and have been applied to a bacterial artificial chromosome (BAC) array comparative genomic hybridization (CGH) platform. The platform is described in detail by Greshock and colleagues (20) and its application and methodology for neuroblastoma CNA detection by Mosse and colleagues (21). Briefly, normalized $\log_2$ intensity ratios were averaged within slide for each BAC clone using the DNAcopy package within Bioconductor.[10] A mean $\log_2$ ratio of $\geq$1.0 was considered a high-level amplification. Amplification of both the *MYCN*-containing BAC and the CTD-2603D17 clone that contains *ODC1* and was used to define coamplification.

A second independent cohort of 265 neuroblastomas from COG with available RNA was studied. Outcome data were available for 209 (79%). Informed consent was obtained from all subjects. Clinical characteristics and RNA/cDNA isolation procedures were previously described (22). *ODC1* and *MYCN* expression was determined by real-time quantitative PCR (Q-PCR). The *β2-microglobulin* gene served as an internal control and the primers and probe sequences for β2-microglobulin and *MYCN* have been reported (22). *ODC1* primer and probe sequences were 5′-GATGACTTTTGATAGTGAAGTTGAGTTGA-3′ (forward primer), 5′-GGCACCGAATTTCACACTGA-3′ (reverse primer), and 5′-CGGATTGC-CACTGATGATTCCAAAGC-3′ (probe). Q-PCR data were collected using a Prism 7700 Sequence Detection System (Applied Biosystems) and the level of target gene expression was determined using the $\Delta\Delta C_t$ method (22). For all tumors in these studies, *MYCN* status was defined as >4-fold copies of *MYCN* compared with a 2p reference probe using fluorescence *in situ* hybridization (FISH).

### Cell Lines and Tissue Culture

Neuroblastoma cell lines were obtained from the Children's Hospital of Philadelphia Cell Line Bank courtesy of Garrett M. Brodeur and have been previously reported (23). Cells were grown in RPMI 1640 (Life Technologies) supplemented with 10% fetal bovine serum, 2 mmol/L L-glutamine, 100 units/mL penicillin, and 100 μg/mL gentamicin. Tissue culture was at 37°C in a humidified atmosphere of 5% $CO_2$ as previously described (24). Cell line transcriptome profiles were obtained using the Affymetrix U133+2 oligonucleotide array and analyzed as above.

### Cell Line *ODC1* Expression

Real-time Q-PCR (Taqman) was used to quantify *ODC1* mRNA. Total RNA (2 μg) was reverse transcribed in a 20 μL reaction using the SuperScript III First-Strand Synthesis System (Invitrogen). The probe and primer set used for *ODC1* detection was Assay-on-Demand Hs00159739_m1 (Applied Biosystems). The genes *SDHA* and *HPRT* served as housekeeping genes for normalization. Triplicate reactions were performed and the mean expression values were used for calculating relative expression.

### Cytotoxicity Assays

Cells were seeded into multiwell sensor microplates at $3 \times 10^4$ per well and allowed to adhere overnight. Cell index was obtained for each test condition in duplicate over 96 h using the real-time cell electronic sensor system (RT-CES, ACEA Biosciences). This label-free dynamic monitoring system uses electrical impedance to quantify viable adherent cell number in real time (25). 2-Difluoromethyl-DL-ornithine (DFMO; Eflornithine) was added to culture medium at a final concentration of 2.5, 5, or 10 μmol/L. DFMO for all studies was generously provided by Patrick Woster (Wayne State University) courtesy of ILEX Pharmaceuticals. All experiments were replicated thrice.

### *TH-MYCN* Mouse Trials

129X1/SvJ mice transgenic for the *TH-MYCN* construct (26–28) were graciously provided by William Weiss (Department of Neurology, University of California at San Francisco, San Francisco, CA) for establishment of *TH-MYCN* breeding colonies in both Philadelphia and Sydney. All studies were approved by the Institutional Animal Care and Utilization Committee at The Children's Hospital of Philadelphia (Philadelphia) and the Animal Care and Ethics Committee of the University of New South Wales (Sydney).

**Preemptive therapy trial (Philadelphia).** *TH-MYCN* hemizygous mice were bred and litters were randomized to water or water with 1% DFMO from birth onward. DFMO passes in breast milk so treated pups received DFMO from birth. After weaning at about day 28, mice continued *ad libitum* water or water with 1% DFMO as initially randomized through day 70. Mice were genotyped from 1-cm tail snip isolated DNA. Primers to detect the human *MYCN* transgene were 5′-CACAAGGCCCTCAGTACCTC-3′ (forward) and 5′-AGGCATCGTTTGAGGATCAG-3′ (reverse). Hemizygous or homozygous transgene status was determined using real-time Q-PCR (Taqman) with the following: TM-MYCNF1 primer, 5′-CGACCACAAGGCCCTCAGT-3′ (within exon 2); TM-MYCNR1 primer, 5′-AGGAGGAACGCCGCTTCT-3′ (exon 3); MYCN probe, FAM-ATCGCTCAGGGTGTCCTCTCCGG-TAMRA; murine B-actinF1 primer, 5′-TGCGTCTGGACTTGGCTG-3′; murine B-actinR1, 5′-TAGCCACGCTCGGTCAGG-3′; and murine B-actin probe, VIC-CGGGACCTGACTGACTACCTCATGA-TAMRA. For each analysis, 10 ng template DNA was used. All unknowns, FISH confirmed homozygous and hemizygous *TH-MCYN* controls, and nontemplate controls were loaded in triplicate. The average transgene dose was calculated using $\Delta\Delta C_t$ and calls were made based on comparison with control values within each run.

Palpation for intra-abdominal tumors was performed thrice weekly. Animals with palpable tumors underwent serial abdominal ultrasonography under isoflurane sedation to determine *in situ* tumor volume using a Vevo660 imaging system with 3D Acquisition and Visualization software (VisualSonics). Mice were screened by experienced animal personnel and sacrificed for pathologic signs of tumor burden (predominantly hunching and poor mobility).

**Delayed treatment trial (Sydney).** The specific characteristics of the Sydney breeding colony of *TH-MYCN* transgenic mice, including their maintenance, genotyping, and tumor incidence and latency, have been described previously (26). Cohorts of mice received plain water or 1% DFMO in their water *ad libitum* from day 25 (postweaning) onward. Animals were abdominally palpated twice weekly by experienced staff. Time to onset of tumor development and time to sacrifice according to well-defined humane end points were determined for all animals (26).

[9] http://www.ncbi.nlm.nih.gov/geo/ (accession number GSE3960).
[10] http://www.bioconductor.org

**Combination chemotherapy treatment in *TH-MYCN* mice.** Homozygous *TH-MYCN* mice with palpable tumors of 5 to 7 mm in diameter ($n \geq 10$ per group) were treated with cisplatin (2 mg/kg, i.p. daily × 5 d; Pharmacia) or cyclophosphamide (20 mg/kg, i.p. daily × 5 d). The control groups were treated with chemotherapy alone, whereas DFMO-treated groups received either continuous 1% DFMO in drinking water after completion of the cisplatin course or 1% DFMO in drinking water simultaneously with cisplatin or cyclophosphamide and continuously thereafter. Animals were sacrificed when tumors recurred, according to well-defined humane end points (26), or otherwise at 140 d of age.

### Tumor Histolopathology and Polyamine Content

Animal tumors and tissues were harvested at sacrifice and fixed in 10% neutral buffered formalin and paraffin embedded for histologic studies as well as flash frozen in liquid nitrogen for metabolic assays. Tissue sections were stained with H&E and assessed histologically by a pathologist (B. Pawel) for confirmation of tumor type, and percentage of necrosis (average of five 40× microscopic fields) and mitotic/karyorrhectic cells (average of five 600× microscopic fields).

For immunohistochemistry, 5-μm sections were stained with antibodies to caspase-3 at a 1:1,000 dilution (R&D Systems) and Ki67 at a 1:1,000 dilution (Santa Cruz Biotechnology) on an Autostainer Plus staining system (DakoCytomation) using standard methods, including microwave antigen retrieval for 5 min in 0.01 mol/L citrate buffer at pH 7.6. Both caspase-3 and Ki67 staining were scored as the percentage of stained tumor nuclei using the average of five 600× microscopic fields.

Tumor tissues were frozen in liquid nitrogen, ground to a fine powder, and stored at −80°C. For polyamine analyses, ground tissues were homogenized in 0.2 N perchloric acid and incubated at 4°C overnight. Dansylated polyamines were separated on a reversed-phase C18 high-performance liquid chromatography column (29). Polyamine values were normalized to the amount of DNA in the tissue extracts.

### Murine Paravertebral Ganglia Studies

To study the *in vivo* effects of perinatal Odc1 inhibition, litters from *TH-MYCN* mice were randomized and treated with 1% DFMO in maternal drinking water as above. Pups were euthanized at postnatal days 0 ($n = 26$), 7 ($n = 40$), and 14 ($n = 26$). Additionally, a cohort of pregnant females received DFMO prenatally from embryonic days 14 to 21 and ganglia from pups were obtained at day 0. Tissues were formalin fixed and paraffin embedded. A histologic audit was performed with each section scored for the presence of >30-cell neuroblast hyperplasia. Animals were *TH-MYCN* genotyped as previously described (30).

Paravertebral sympathetic ganglia were dissected from normal and *TH-MYCN* mice at postnatal day 14 and cultured for 3 to 5 d as described previously (27). DFMO (1 mmol/L) was added to half the wells for 7 d. On day 5, cells were washed twice and 10 μg/mL anti-nerve growth factor (NGF) antibody (Chemicon) or isotype control (Cedarlane Laboratories) was added to alternate wells for 48 h. The number of neurons surviving withdrawal of NGF was quantitated using immunofluorescent staining for the neuron-specific marker βIII-tubulin, expressed as a percentage of neurons positive for βIII-tubulin before and after NGF withdrawal.

For Odc1 immunohistochemistry, cells from murine ganglia were cultured as described (27) and then treated with 1 mmol/L DFMO for 7 d. Medium was replaced every 2 to 3 d with complete medium containing anti-NGF and DFMO. Cells were fixed with 4% formaldehyde (20 min at room temperature) followed by methanol permeabilization (20 min at room temperature). Immunofluorescent staining was performed using a mouse Odc antibody (clone MP16-2; 1:25 dilution; Sapphire Biosciences) or isotype control in conjunction with the Vector Labs M.O.M kit (Australian Laboratory Services). DFMO competitively inhibits binding of this antibody to Odc1 (31). Cells were imaged using an Axioplan 2 microscope (Zeiss) using a SensiCam charge-coupled device camera (PCO Imaging).

### Statistical Analyses

Pearson's correlation coefficients were calculated to assess gene expression correlations. Two-tailed Student's $t$ test was used to test significance unless otherwise stated. Survival analyses were performed according to the method of Kaplan and Meier (32) with SEs according to Peto and Peto (33). Comparisons of outcome between subgroups were performed by a two-sided log-rank test. Event-free survival (EFS) time was calculated as described previously (22) and death was the only event considered for the calculation of overall survival (OS) time. A continuous range of *ODC1* Q-PCR values was used in outcome analyses. To categorize expression as either high or low, the following cut-points were tested: the mean, median, upper quartile, and upper decile values (34). The cut-point that maximized the difference in EFS between the two groups was selected, and that cut-point was applied to analyses of the overall cohort as well as the subgroups.

## Results

***ODC1* expression correlates with survival in neuroblastoma.** Odc1 is rate limiting for polyamine biosynthesis, a bona fide oncogene, and direct *MYCN* target. We therefore compared *ODC1* mRNA expression with *MYCN* gene status, *MYCN* expression, and outcome in a large cohort of neuroblastoma patients. *ODC1* expression was significantly higher in *MYCN*-amplified tumors (Fig. 1*A*) and strongly correlated with *MYCN* expression ($r = 0.80$; $P < 0.0001$). EFS for patients with high *ODC1* expression (defined as the upper decile and determined by an optimal cut-point analysis) was significantly poorer than that of patients with low *ODC1*, with 5-year rates of 38 ± 11% and 76 ± 3% (Fig. 1*B*). Similarly, worse OS was associated with high *ODC1* ($P < 0.001$). High *ODC1* was associated with worse EFS and OS when the groups were dichotomized around the mean, median, or upper quartile as well ($P < 0.05$ for each). In patients with stage IV metastatic disease, high *ODC1* expression was again associated with reduced EFS or OS (Fig. 1*C*).

Because *MYCN* amplification has a negative influence on survival through regulation of numerous target genes (in addition to *ODC1*), we assessed tumors without *MYCN* amplification. Again, high *ODC1* was associated with a worse EFS and OS, with 5-year EFS rates of 43 ± 19% compared with 80 ± 3% (Fig. 1*D*), suggesting a role for *ODC1* in promoting an aggressive phenotype (for dichotomization at the mean, median, or upper quartile, the $P$ value was again <0.05). In nonamplified neuroblastomas, there is no correlation between *MYCN* expression and outcome, so it is unlikely that this is a surrogate for *MYCN* activity (30). To assess the independent prognostic significance of *ODC1* while controlling for known powerful prognostic factors such as tumor stage (stages I, II, and IVS versus III and IV), age at diagnosis (<1 versus ≥1 year), and *MYCN* status, these factors were tested in a Cox proportional hazards model with dichotomized *ODC1* expression. The addition of *ODC1* expression by itself did not add independent significance to this highly prognostic model.

**Neuroblastomas with *MYCN* amplification show coordinate pathway alterations that enhance polyamine biosynthesis.** To further explore polyamine metabolism (see pathway, Fig. 2*A*), we mined transcriptome profiles from neuroblastomas of diverse risk classes (17). As predicted, *MYCN* and *ODC1* mRNAs were significantly higher in HR-A tumors in comparison with all other groups (Fig. 2*B*). Odc1 is additionally regulated by antizymes (*OAZs*) that direct its degradation, whereas *OAZIN* inhibits this activity. *OAZ2* was significantly reduced in HR-A neuroblastomas, further promoting Odc activity. Notable were alterations in numerous polyamine regulators in HR-A tumors, all in a direction promoting biosynthesis. Each prosynthetic enzyme was up-regulated (confidence level, >0.95), whereas there was a reduction in *SMOX* that catabolizes polyamines (note, no *PAOX* probe sets

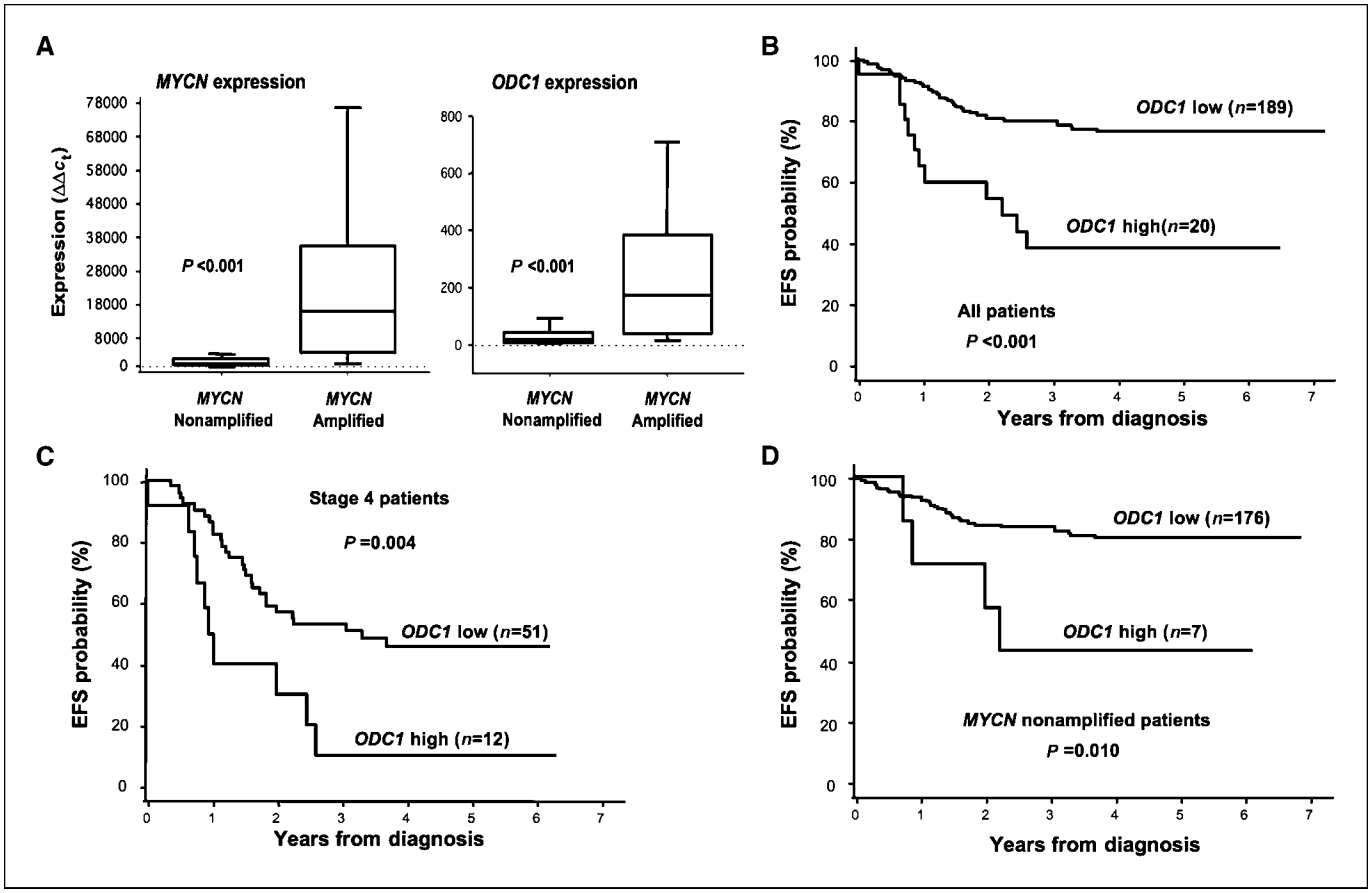


**Figure 1.** *ODC1* expression is correlated with *MYCN* and inversely correlated with survival. *A, MYCN* and *ODC1* expression by real-time Q-PCR in a set of 265 primary neuroblastomas stratified by *MYCN* amplification status. *Columns,* mean of triplicate assays; *bars,* SE. Two-tailed *P* values are indicated. EFS curves for (*B*) all 209 neuroblastoma patients with outcome data available, (*C*) the subset of metastatic stage IV patients, and (*D*) the subset with tumors without *MYCN* amplification ($n$ = 183), dichotomized around the upper decile for *ODC1* expression (with *P* values using the method of Kaplan-Meier). EFS and OS were also significantly reduced in the high *ODC1* cohort when dichotomized at the mean, median, or upper quartile.

were on the array). Together, these data show systematic alterations in polyamine metabolism correlated with *MYCN* amplification. High-risk tumors without *MYCN* amplification (HR-NA) also had higher *ODC1* and reduced *OAZ2* compared with low- and intermediate-risk tumors, suggesting pathway enhancement in these tumors as well.

*ODC1, SRM*, and *AMD1* have been posited as Myc targets (Myc Cancer Gene Database)[11] and our data support this. *ODC1* was strongly correlated with *MYCN* across the entire cohort ($r$ = 0.53; $P$ < 0.0001; Fig. 2*C*). *SRM* and *AMD1* yielded similar correlations ($r$ = 0.30; $P$ = 0.001 and $r$ = 0.59; $P$ = 0.001, respectively). *SMS*, despite no prior evidence as a *MYC* target, had the strongest correlation ($r$ = 0.69; $P$ < 0.0001), whereas *OAZ2* was inversely correlated ($r$ = −0.42, $P$ < 0.0001; see Supplementary Fig. S1), although not a previously identified repressed target. Thus, *MYCN*-amplified neuroblastomas directly or indirectly promote polyamine pool expansion through coordinate alteration of multiple polyamine regulators through mechanisms that may include *de novo* transcriptional initiation or mRNA stability.

The correlation between *MYCN* and *ODC1* expression was less evident in tumors with *MYCN* amplification (compared with other bona fide *MYCN* targets) due to the presence of outliers with exceptionally high *ODC1* (Fig. 2*C*). *ODC1* maps ~5.5 Mb telomeric to *MYCN* (2p24) using the University of California at Santa Cruz Genome Browser coordinates. We sought whether *ODC1* was coamplified with *MYCN* as has been reported (35). Eighty of the 101 tumors had DNA available for determination of *MYCN* and *ODC1* genomic copy number using a BAC array CGH platform (21). No tumors without *MYCN* amplification ($n$ = 64) had *ODC1* amplification. Sixteen *MYCN*-amplified tumors (by FISH) were confirmed to have high-level *MYCN* amplification using array CGH. Three of these (19%) had high-level *ODC1* coamplification and each was an outlier with extremely high *ODC1* expression (Fig. 2*C, arrowheads*; the fourth outlier did not have DNA for CNA determination). Thus, a subset of neuroblastomas coamplifies both the transcriptional regulator (*MYCN*) and target gene (*ODC1*) to augment effects on polyamine biosynthesis, a putative "amplification loop" that has not been previously postulated.

**Disabling *ODC1* in neuroblastoma cell lines inhibits proliferation.** Across 26 neuroblastoma cell lines, there was a trend for higher *ODC1* with *MYCN* amplification [$P$ = 0.10; $P$ = 0.06 if NBL-S with prolonged MycN half-life (36) is included in the "amplified" cohort; Supplementary Fig. S2]. We assessed Odc1 inhibition *in vitro* using DFMO, an irreversible Odc inhibitor. DFMO-mediated growth inhibition correlated with *ODC1* mRNA expression and proliferative rates (Fig. 3*A*), was apparent by early

[11] http://www.myccancergene.org

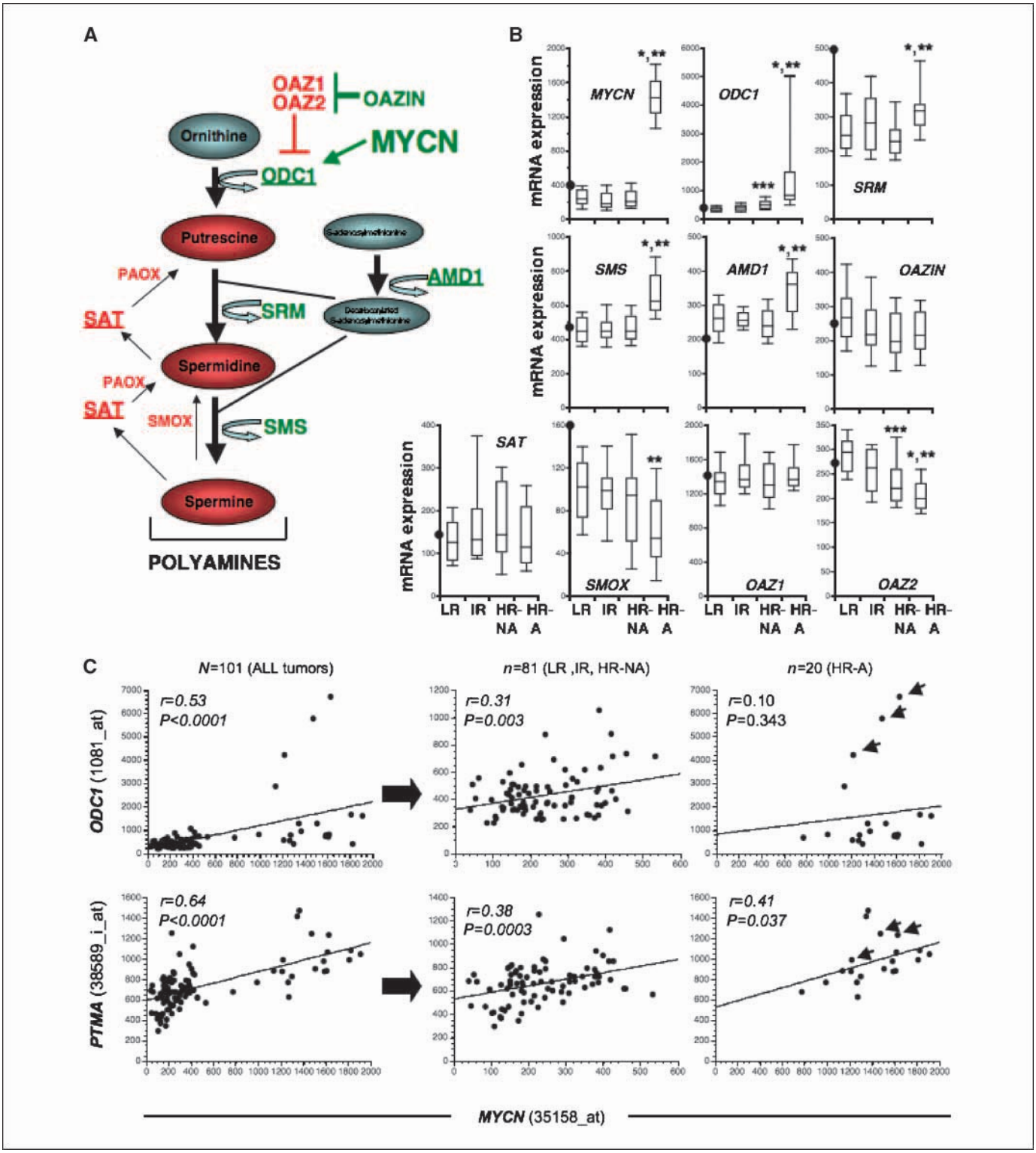


**Figure 2.** Polyamine regulation in neuroblastoma. *A,* polyamine metabolism: polyamines (putrescine, spermidine, and spermine) are synthesized from ornithine through decarboxylation and condensative processes. Synthetic (*green*) and catabolic (*red*) enzymes are shown. Underlined enzymes are highly regulated with the shortest half-lives of any mammalian enzymes. *ODC1,* ornithine decarboxylase; *AMD1, S*-adenosylmethionine decarboxylase; *SRM,* spermidine synthetase; *SMS,* spermine synthetase; *SAT,* spermine/spermidine-*N*-acetyltransferase; *SMOX,* spermine oxidase; *OAZ1,* ODC antizyme 1; *OAZ2,* ODC antizyme 2; *OAZIN,* ODC antizyme inhibitor. *B,* polyamine regulator expression in primary neuroblastomas: *LR,* 28 low-risk tumors; *IR,* 21 intermediate-risk tumors; *HR-NA,* 32 high-risk tumors without *MYCN* amplification; *HR-A,* 20 high-risk tumors with *MYCN* amplification. *, differential expression between HR-A and HR-NA; **, differential expression between HR-A and all others; ***, differential expression between HR-NA and LR and IR (all with a confidence level >0.95 using PaGE analyses). *Filled circle on Y axis,* fetal brain (control) expression. *C,* correlation between *ODC1* and *PTMA* with *MYCN* expression using representative probe sets. *Left,* all 101 tumors; *right,* segregate HR-A tumors from the other groups. Pearson's correlation coefficient and *P* values are given. *Arrowheads,* the three tumors that have both high-level *MYCN* and *ODC1* coamplification.

time points (48 hours), and was seen in cells both with and without *MYCN* amplification. Indeed, Affymetrix expression data for neuroblastoma cell lines and fetal brain cDNA show up-regulation of polyamine synthetic enzymes and down-regulation of catabolic enzymes in nonamplified cells (Fig. 3*B*). This growth inhibition is not surprising as most cell types show cytostasis when Odc is inhibited *in vitro*, including neuroblasts (37). Tissue culture conditions do not provide the same rescue opportunities present to cells depleted of polyamines *in vivo*, where many markedly increase polyamine uptake, an option not present in polyamine-poor culture medium. We therefore focused on polyamine depletion effects *in vivo*.

**Disabling Odc1 prevents *MYCN*-mediated oncogenesis.** We determined the effect of disabling Odc (to impede polyamine

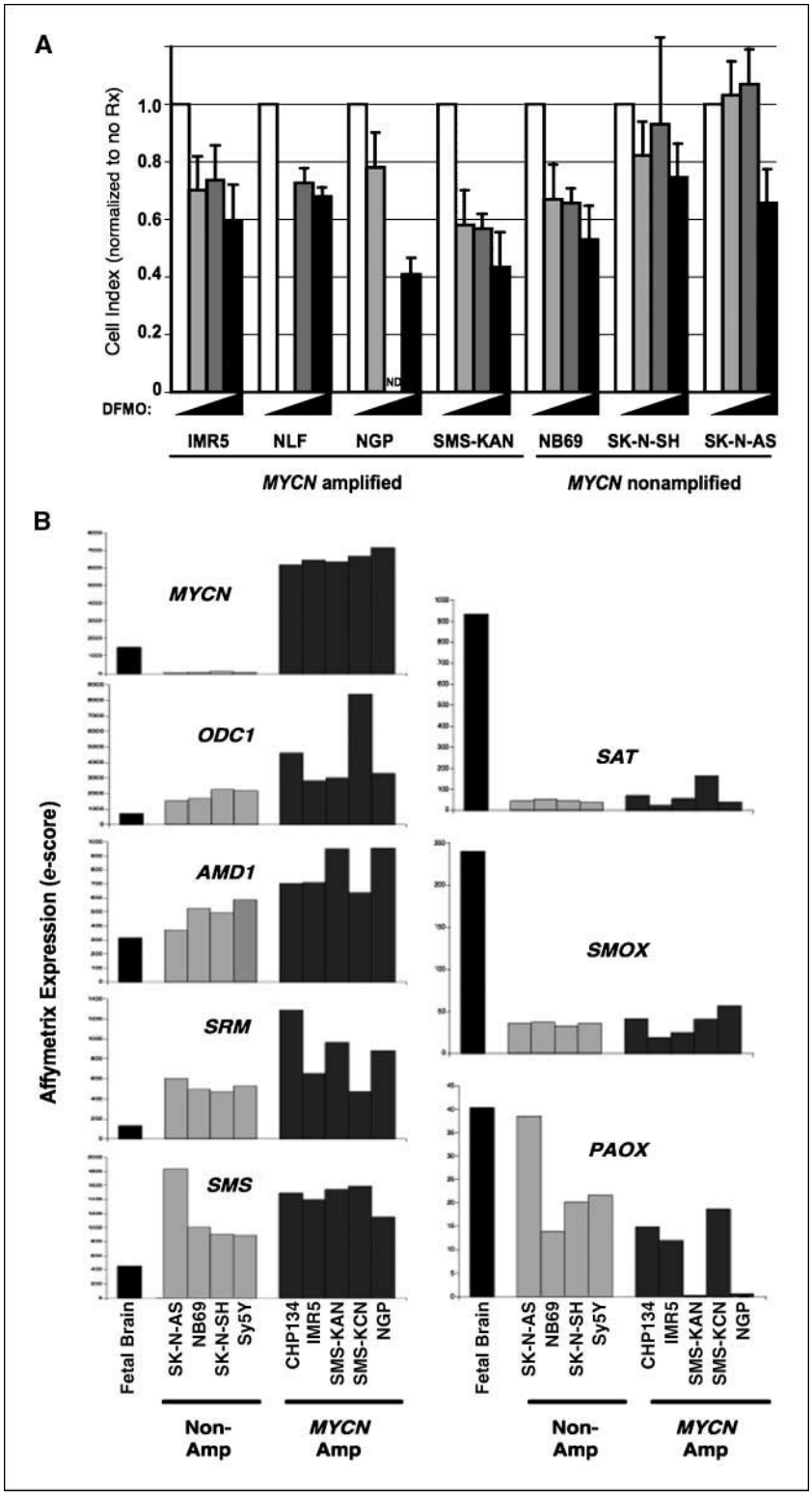


**Figure 3.** Polyamine dependence in neuroblastoma cell lines. *A,* DFMO-mediated growth inhibition *in vitro*. Cell index, proportional to the viable cell number, was obtained with the RT-CES platform. Viable cell number following short-term exposure to DFMO is shown normalized to no treatment at 72 h. *White columns,* control; *light gray columns,* 2.5 mmol/L DFMO; *dark gray columns,* 5 mmol/L DFMO; *black columns,* 10 mmol/L DFMO. Triplicate wells are assessed for each experiment and multiple experiments are done for each condition. *Bars,* SD. *B,* Affymetrix expression (*e*-score) for polyamine regulatory enzymes in neuroblastoma cell lines, segregated by *MYCN* status and compared with fetal brain cDNA as a normal reference. Both amplified and nonamplified cells have expression alterations in a direction promoting polyamine expansion (more pronounced in the amplified cells).

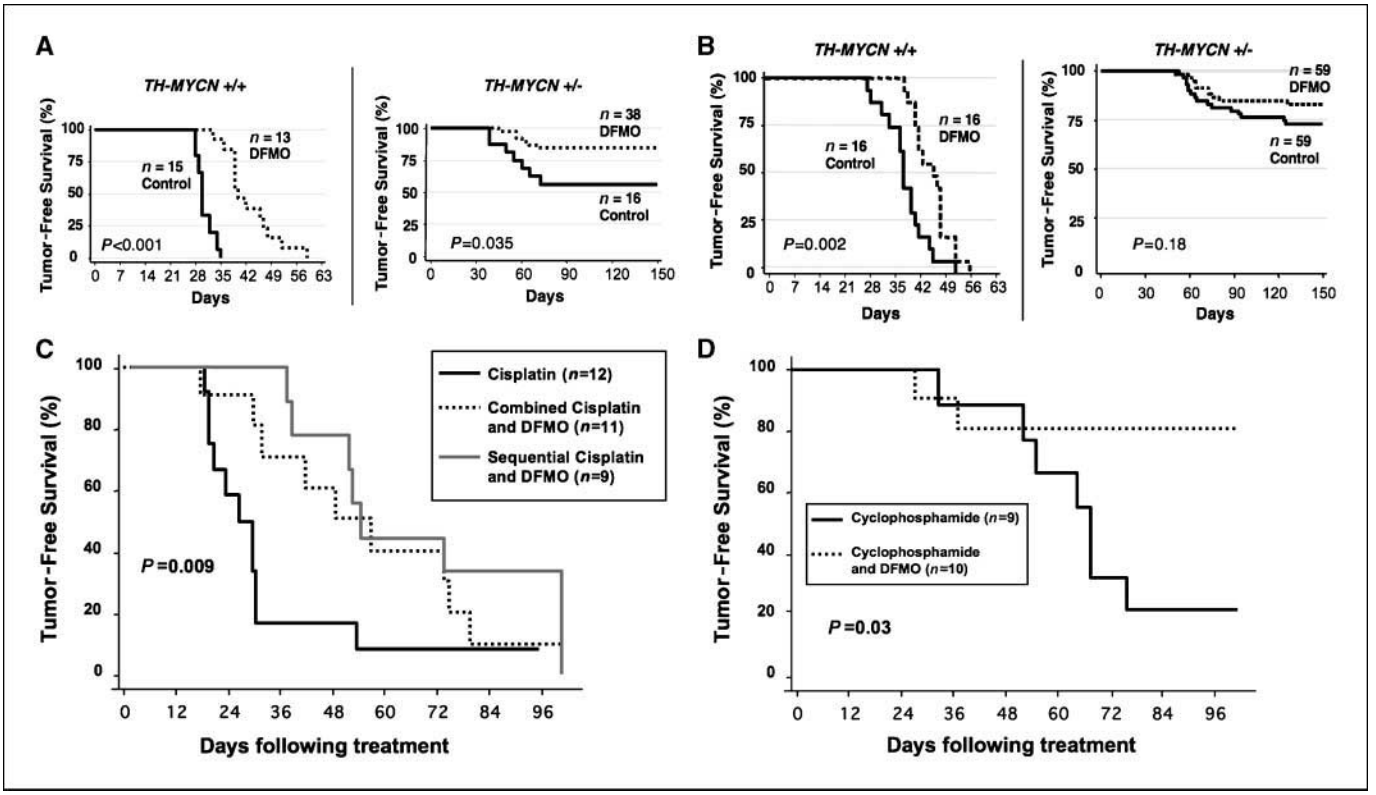


**Figure 4.** Extended tumor-free survival in neuroblastoma-prone mice treated with DFMO. *A,* tumor-free survival curves for homozygous (*TH-MYCN +/+*) or hemizygous (*TH-MYCN +/−*) mice stratified by DFMO therapy. DFMO-treated mice (*dashed lines*) received DFMO from birth onward (preemptive treatment trial). DFMO therapy was stopped at day 70 in tumor-free mice. *B,* delayed treatment trial: *TH-MYCN* homozygous and hemizygous mice were randomized to DFMO (*dashed lines*) or control (*solid lines*) following weaning at day 25. Tumor-free survival for *TH-MYCN* homozygous mice with advanced tumor from the time of treatment with (*C*) cisplatin alone (*black line*), cisplatin followed by DFMO (*gray line*), or cisplatin administered simultaneously with DFMO (*dashed line*) or (*D*) cyclophosphamide alone (*solid line*) or combined with DFMO (*dashed line*). *P* values using the method of Kaplan-Meier are shown.

synthesis) on both tumor initiation and progression using a *MYCN* transgenic mouse model. Mice homozygous for a neural crest–targeted *MYCN* transgene (*TH-MYCN*) develop tumors with complete penetrance, whereas hemizygous *TH-MYCN* mice have reduced ( ~ 30%) tumor penetrance (27, 28). Tumors develop within hyperplastic rests that are transiently present even in wild-type animals (27). Their number and persistence correlate with tumor penetrance and *MYCN* dosage. Tumors share biochemical features and orthologous genomic alterations with human neuroblastomas, suggesting preferred secondary pathways are recapitulated (28, 38, 39). Thus, the model provides a platform for evaluating biopathway targeted therapies (40).

We evaluated whether Odc activity was required for *MYCN*-initiated oncogenesis by treating mice with DFMO from birth. All mice homozygous for the transgene (highest *MYCN*) developed tumors; however, tumor latency (mean, 31 ± 2 versus 43 ± 7 days; $P < 0.001$) and OS (mean, 43 ± 4 versus 59 ± 9 days; $P < 0.001$) were markedly extended by DFMO (Fig. 4*A*). Moreover, hemizygous mice (high *MYCN*) were protected from tumor initiation. Seven of 16 untreated hemizygous mice (44%) developed tumors, consistent with the penetrance observed historically, whereas only 6 of 38 DFMO-treated mice (16%) developed tumors ($P = 0.035$). Importantly, DFMO was removed at day 70, yet no tumors arose beyond this time point. This is consistent with a finite vulnerable period for embryonal oncogenesis and suggests that transiently inhibiting Odc1 provides long-lasting tumor protection.

Delaying Odc inhibition until after tumor onset also had a measurable effect. In a second trial, DFMO therapy was initiated after weaning when small tumors are invariably present in homozygous animals and in the majority of hemizygous animals (27). DFMO treatment of homozygous mice again inhibited progression (time to palpable tumor burden: mean, 47.5 ± 1.3 versus 38.6 ± 1.5 days) and time to death (mean, 49.2 ± 1.3 versus 42.6 ± 1.2 days; $P = 0.001$; Fig. 4*B*). Delayed DFMO treatment in hemizygous mice did not reduce penetrance (as the majority of tumors were present before therapy), yet there was a modest trend toward tumor inhibition based on a reduction in penetrance and extended tumor-free survival and OS.

**DFMO enhances the therapeutic effect of chemotherapy.** DFMO has been shown to induce cell cycle arrest in neuroblasts (37) and therefore may interfere with chemotherapy effects. We assessed Odc inhibition in combination with cisplatin, vincristine, or cyclophosphamide, first-line agents with high single-agent activity in neuroblastoma. *TH-MYCN* homozygous mice with palpable intra-abdominal tumors (75–150 $mm^3$) were treated with the chemotherapeutic alone or in combination with DFMO. Cisplatin induced transient tumor regression with a mean latency to recurrence of 32 days. DFMO started concurrently or following cisplatin and continued thereafter did not interfere with cisplatin-induced regression and led to an extended relapse-free survival ($P < 0.01$; Fig. 4*C*). Similar findings were obtained using vincristine (data not shown), and a more marked augmentation of chemotherapy efficacy was seen with cyclophosphamide, where

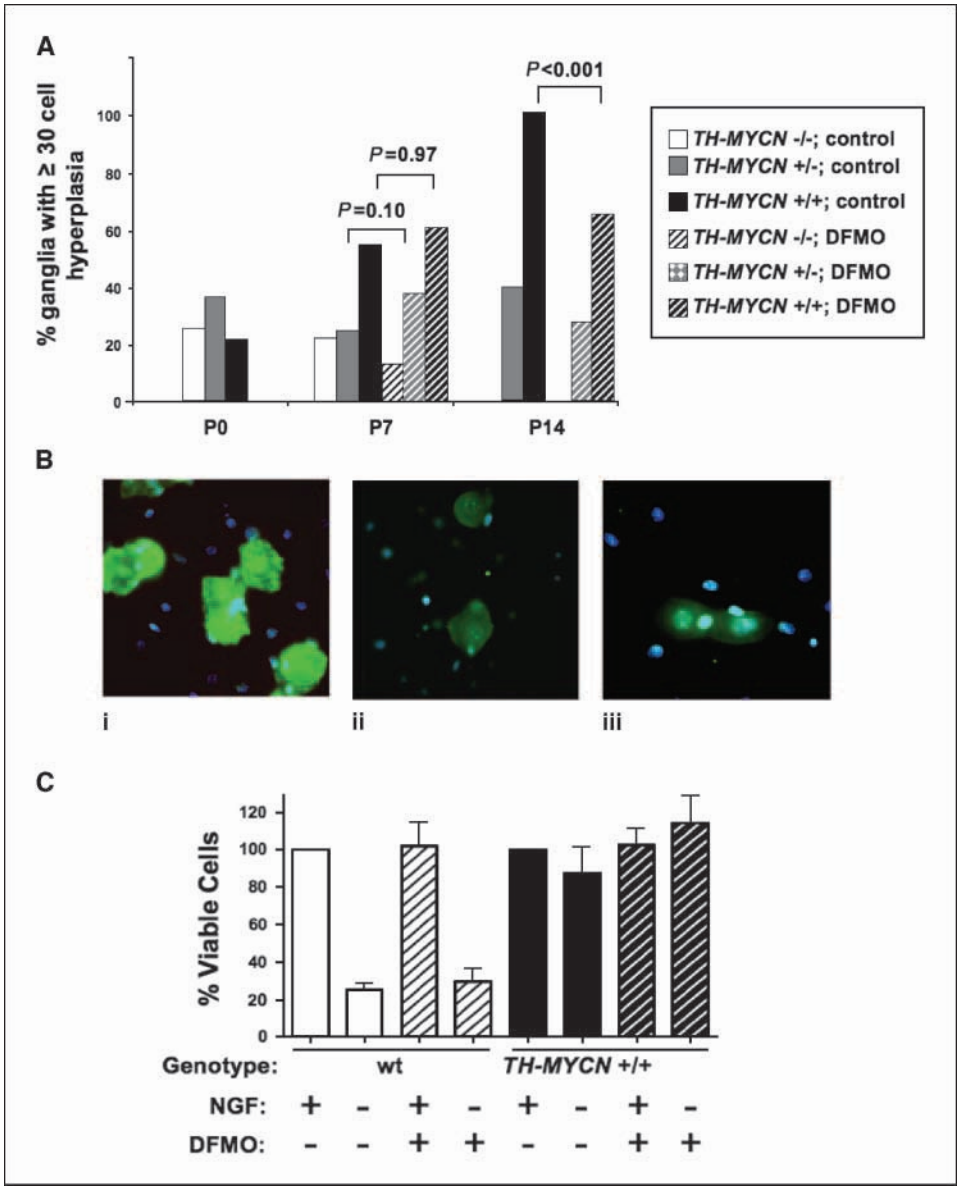


**Figure 5.** DFMO inhibits Odc activity and *MYCN*-driven hyperplasia but does not revert the apoptosis resistance provided by *MYCN*. *A,* neuroblast hyperplasia following DFMO-mediated Odc1 inhibition in *TH-MYCN* homozygous (+/+) or hemizygous (+/−) mice, and wild-type (−/−) littermates. The percentage of ganglia with ≥30-cell neuroblast hyperplasia at each time point is shown. DFMO-treated mice differed significantly from untreated mice among homozygotes at P14 ($P < 0.001$) but not hemizygote or normal pups at either time point. *B,* relative Odc1 activity in normal ganglia following DFMO-mediated inhibition. Protein expression was detected using an Odc activity-specific antibody (clone MP16-2). Green fluorescence represents uninhibited (active) Odc1; blue fluorescence is 4′,6-diamidino-2-phenylindole nuclear stain. *i,* untreated ganglia cells; *ii,* DFMO-treated cells; *iii,* isotype control. *C,* relative ganglia cell survival *in vitro*, both before or after NGF withdrawal in normal (*white columns*) or *TH-MYCN* homozygote (*black columns*) cells, in the presence (*hatched columns*) or absence of 1 mmol/L DFMO. Disabling Odc1 activity with 1 mmol/L DFMO did not diminish the survival advantage governed by *MYCN* in ganglia cells from homozygote animals.

cyclophosphamide alone resulted in long-term cure of ~20% of neuroblastoma-bearing mice. Concurrent administration of DFMO with cyclophosphamide increased OS to 80% ($P = 0.03$; Fig. 4*D*).

We noted no overt toxicity attributable to DFMO therapy in these trials. Wild-type mice receiving DFMO from birth weighed less than untreated littermates following weaning (~day 28), yet they gained weight at the same rate or better thereafter, despite ongoing DFMO exposure (average weight gain of 0.45 g/wk in DFMO-treated mice versus 0.28 g/wk for control mice between weeks 14 and 20; $P = 0.12$; Supplementary Fig. S3). Mice receiving DFMO delayed until after weaning showed modest growth inhibition through 5 months of life compared with untreated animals (weight gain of 0.92 ± 0.04 versus 1.05 ± 0.04 g/wk; $P = 0.034$).

**Odc activity is not required for *MYCN*-mediated death resistance.** Tumors in *TH-MYCN* mice arise within hyperplastic rests in sympathetic ganglia. These are transiently present in wild-type mice but are increased in number and persist longer in a *MYCN* dose-dependent manner (27). We assessed the effect of DFMO on this process by performing a histologic audit. Prenatal DFMO treatment of pregnant mothers from embryonic days 14 to 21 did not affect the incidence of hyperplasia noted at day 0 (data not shown). Postnatal DFMO treatment of newborn pups did not have a demonstrable effect on neuroblast hyperplasia by day 7; however, by day 14, homozygote mice (highest *MYCN*) treated with DFMO showed a significant reduction (Fig. 5*A*). Together with *in vivo* data, this suggests that Odc activity is not required for basal neuroblast hyperplasia; however, *MYCN* supported maintenance and progression to tumor is at least partially Odc dependent.

*MYCN* not only drives cell cycle entry but also protects against deprivation-induced apoptosis in *TH-MYCN* neural cells. Cultured perinatal ganglia from *TH-MYCN* mice show resistance to NGF withdrawal (27) analogous to that seen in postmitotic sympathetic neurons (41). Paravertebral ganglia from untreated normal and *TH-MYCN* homozygote mice at day 14 were cultured in the presence of NGF with or without DFMO for 7 days, after which NGF was withdrawn. Although DFMO-mediated Odc inhibition was supported using a conformation-specific antibody (Fig. 5*B*), there was

no effect on the death resistance of ganglia cells, showing that Odc-mediated polyamine synthesis was not a critical component of *MYCN*-mediated apoptosis resistance (Fig. 5*C*).

**Neuroblastomas arising under DFMO may circumvent the polyamine depletion barrier.** We assessed whether tumors arising under Odc inhibition overcame this blockade or took an alternative route to transformation less dependent on polyamines. DFMO-treated and untreated mice developed cellular tumors that were undifferentiated (with the exception of one lymph node that had fibrillary neuropil) similar to poorly differentiated human neuroblastoma. DFMO-treated tumors had larger cells with reduced hemorrhage and necrosis but no differences in mitosis/karyorrhexis index (Fig. 6*A*). Tumors were notable for the large percentage of cycling cells ($Ki67^+$) and caspase activation, although neither differed between groups. Serial ultrasonography in homozygous *TH-MYCN* mice confirmed similar tumor volume at the time of ascertainment (mean, 227 $\pm$ 61 $mm^3$ versus 232 $\pm$ 64 $mm^3$; $P = 0.83$), although tumors arose later in DFMO-treated mice. Tumors grew at similar rates ($\Delta$volume/week of 166 $\pm$ 68 $mm^3$ versus 156 $\pm$ 79 $mm^3$ with DFMO; $P = 0.75$) and lethality. Thus, aside from being delayed in onset, DFMO-treated tumors manifested a similar aggressive phenotype in homozygous mice.

Polyamine assays from tumors harvested at culling showed reduced putrescine in DFMO-treated tumors, a trend toward reduced spermidine and no effect on spermine (Fig. 6*B*). These effects are consistent with experimental models of DFMO-induced Odc inactivation (42), including effects on neuroblastoma cell lines (37), and support that polyamine depletion is at least partially maintained. However, maintenance of spermidine and spermine through enhanced polyamine uptake, compensatory Amd1 induction, or altered metabolism cannot be formally excluded as a mechanism for circumventing the polyamine depletion barrier. Further studies are ongoing to determine whether neuroblastomas circumvent Odc inactivation to support polyamine homeostasis or take an alternate route to oncogenesis.

## Discussion

Most children with high-risk neuroblastoma die from tumor progression and innovative treatment approaches are needed (16, 43). We show that neuroblastomas, particularly those with *MYCN* amplification, have altered polyamine metabolism and may be vulnerable to therapeutic polyamine depletion. Although *MYCN* amplification has long been associated with poor outcome (1, 2), the transcriptional targets governing this remain elusive as *MYCN* regulates thousands of genes (7). We show that *MYCN* amplification is correlated with deregulation of numerous enzymes that drive polyamine expansion, and such concerted alterations may be a hallmark of *MYC* oncogenesis (15). Odc1 is rate limiting in this pathway, and importantly, we show that its biochemical inhibition alone has measurable consequences on tumor progression in a transgenic model.

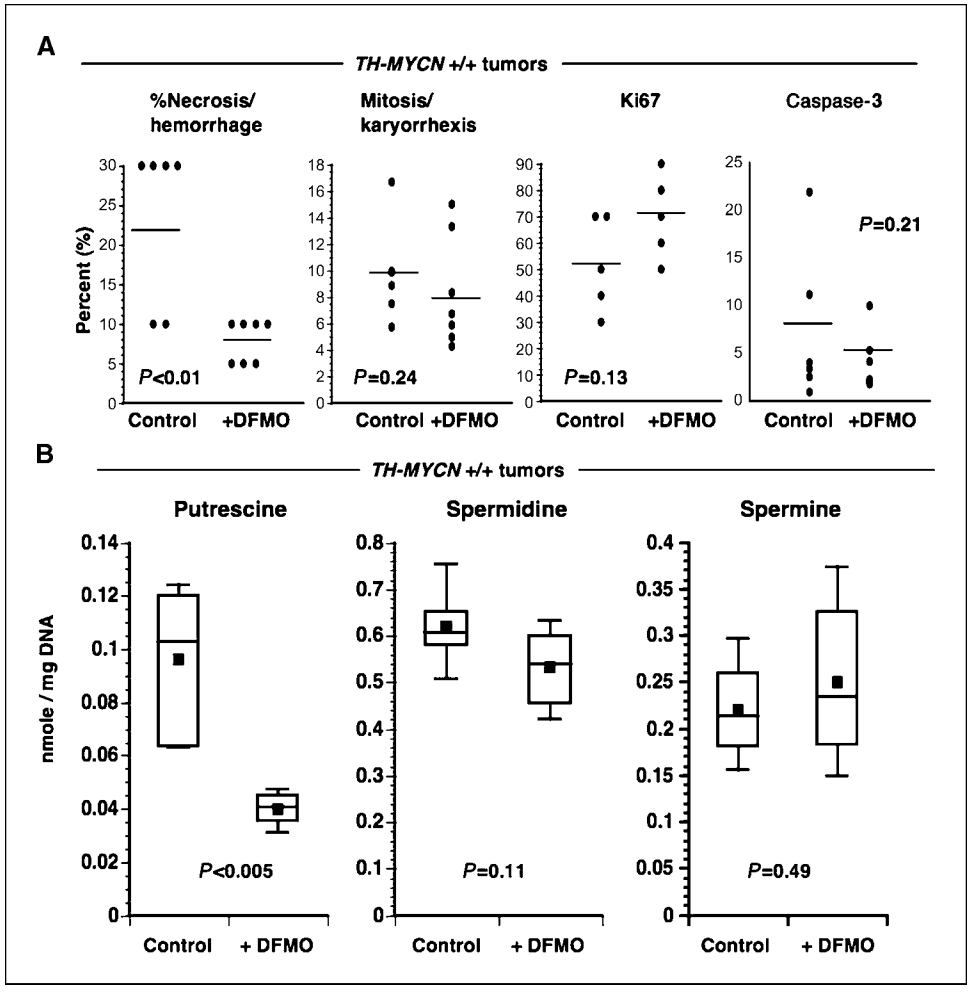


**Figure 6.** Neuroblastomas arising under Odc blockade differ histologically but maintain partial polyamine depletion. Analysis of tumors arising in TH-MYCN +/+ mice with or without polyamine depletion imposed by Odc1 inhibition. *A,* DFMO therapy led to tumors with reduced necrosis or hemorrhage as well as larger cell size but no significant alterations in mitosis/karyorrhexis index, proliferation (Ki67 staining), or apoptosis (activated caspase-3 staining). *B,* evidence for Odc inhibition was apparent by significantly reduced putrescine and a trend toward spermidine reduction in DFMO-treated mice ($n = 6$ per group). This pattern supports an on-target effect of DFMO, although partial circumvention of polyamine synthesis inhibition through uptake of spermidine or spermine cannot be excluded.

Whereas *MYCN*-amplified tumors deregulate diverse polyamine enzymes, high-risk tumors without *MYCN* amplification also have elevated *ODC1* and reduced Odc antizyme (*OAZ2*). Deregulation of this rate-limiting step in polyamine biosynthesis may provide a therapeutic vulnerability here as well. This is supported by demonstration that polyamine regulator expression in *MYCN*-nonamplified cells parallels those for amplified cells, and by *in vitro* data showing DFMO-mediated growth inhibition in nonamplified cells. Of interest, we defined *MYCN* and *ODC1* high-level coamplification in a subset of *MYCN*-amplified tumors associated with markedly elevated *ODC1* expression. As lesser copy number gain of the *ODC1* locus (2p25) is reported in half of high-risk neuroblastomas without *MYCN* amplification (21), we speculate that *ODC1* gene dosage gain is a potential mechanism for pathway up-regulation in this subset. Alternative *MYC* deregulation in high-risk neuroblastomas may also transcriptionally drive *ODC1* expression (4, 5). Importantly, we show that *ODC1* expression is inversely correlated with survival in a large validation cohort even in tumors lacking *MYCN* amplification. Together, these data suggest that polyamine depletion strategies may be more broadly effective against high-risk tumors rather than selectively synthetic lethal for *MYCN*-amplified tumors.

Myc genes induce *Cks1*, a component of the $SCF^{Skp2}$ E3 ubiquitin ligase complex that degrades $p27^{Kip1}$ (44). Because Odc is required both for Myc induction of Cks1 (44) and for polyamine biosynthesis, its activity licenses cell cycle entry at multiple steps. *In vitro*, Odc inhibition causes polyamine depletion and increased $p27^{Kip1}$ and Rb hypophosphorylation with $G_1$ arrest in neuroblasts (37). *In vivo*, we show that Odc activity is not required for basal hyperplastic rest formation (preneoplastic) nor neuroblast resistance to deprivation-induced apoptosis. However, Odc supports hyperplastic rests and promotes their oncogenic conversion. It is likely that DFMO-enforced growth arrest alters the stoichiometry of cycling cells within the peripheral sympathetic compartment to impede tumor initiation.

This selective pressure can prevent tumor onset in *TH-MYCN* hemizygous mice, in which neuroblastoma initiation requires *MYCN* transgene amplification, indicating a higher threshold of *MYCN* permissive for oncogenesis (27). Of greater interest is that transient Odc inhibition through day 70 is capable of providing durable tumor protection. This contrasts with Eμ-*MYC* mice where DFMO withdrawal leads to lymphomagenesis at the expected interval from treatment cessation (15). This is consistent with a finite window for embryonal tumorigenesis beyond which the specific tissue milieu may be incapable of supporting transformation and suggests that chronic Odc inhibition may not be required for sustained therapeutic benefit.

In homozygous *TH-MYCN* mice, disabling Odc from birth delays but does not prevent tumors. The polyamine depletion barrier imposed by Odc inactivation may be bypassed as only putrescine remains depressed and the rate of end-stage tumor progression is reminiscent of untreated animals. DFMO-mediated Odc inhibition is often accompanied by compensatory Amd1 up-regulation that may partly compensate. Alternatively, Odc inhibition may force premalignant neuroblasts to adopt an alternate pathway to transformation, as has been shown for lymphomas arising in Eμ-MYC:Odc+/− mice (15). Still, Odc inhibition after tumor onset delays progression and augments sensitivity to cytotoxic stressors, providing clinical relevance to these studies.

The utility of therapeutic polyamine depletion has been limited to date (14). However, DFMO doses sufficient to inhibit Odc are well tolerated chronically and polyamine depletion as an anticancer strategy is in the midst of a reevaluation. Newer targeted agents are under development, including those that inhibit polyamine uptake from extracellular sources or target additional regulatory enzymes (45–47). That DFMO augments chemotherapy efficacy in our model allays concerns that enforced growth arrest via polyamine depletion will subvert traditional chemotherapeutics. This is reassuring as the entry of polyamine depletion agents into the clinic would likely be in concert with conventional cytotoxics. Interestingly, cisplatinum has been shown to alter *AMD1, ODC1, SRM*, and *SAT* in directions that antagonize polyamine synthesis (48). Yet, the dramatic responses with vincristine or cyclophosphamide and DFMO, including improved OS rates, suggest that this effect does not result from a unique synergistic opportunity provided by platinators alone. Taken together, our data strongly support that polyamine depletion may provide an important addition to the neuroblastoma armamentarium and perhaps other embryonal malignancies governed by *MYC*. Potentiation of these effects with complimentary polyamine-targeted agents may further improve efficacy and deserve further evaluation.

## Disclosure of Potential Conflicts of Interest

No potential conflicts of interest were disclosed.

## Acknowledgments

Received 12/28/2007; revised 7/15/2008; accepted 8/31/2008.

**Grant support:** NIH grants CA97323 (M.D. Hogarty) and CA070739 (S.K. Gilmour), Richard and Sheila Sanford Chair in Pediatric Oncology (M.D. Hogarty), National Health and Medical Research Council Australia (M.D. Norris, M. Haber, and G.M. Marshall), Cancer Institute New South Wales (M.D. Norris, M. Haber, and G.M. Marshall), and Cancer Council New South Wales (M.D. Norris, M. Haber, and G.M. Marshall).

The costs of publication of this article were defrayed in part by the payment of page charges. This article must therefore be hereby marked *advertisement* in accordance with 18 U.S.C. Section 1734 solely to indicate this fact.

We thank COG for providing tumor specimens; Patrick Woster and ILEX Pharmaceuticals for DFMO; William Weiss (University of California at San Francisco) for *TH-MYCN* mice; Qun Wang for Affymetrix data set assistance; Edward Attiyeh, Sharon Diskin, and Yael Mosse for array CGH analyses; and Rosalind Barr, Eric Rappaport, and the Nucleic Acids and Protein Core facility at the Children's Hospital of Philadelphia for technical assistance.

## References

1. Brodeur GM, Seeger RC, Schwab M, Varmus HE, Bishop JM. Amplification of N-myc in untreated human neuroblastomas correlates with advanced disease stage. Science 1984;224:1121–4.
2. Seeger RC, Brodeur GM, Sather H, et al. Association of multiple copies of the N-myc oncogene with rapid progression of neuroblastomas. N Engl J Med 1985;313:1111–6.
3. Perez CA, Matthay KK, Atkinson JB, et al. Biologic variables in the outcome of stages I and II neuroblastoma treated with surgery as primary therapy: a children's cancer group study. J Clin Oncol 2000;18:18–26.
4. Kohl NE, Kanda N, Schreck RR, et al. Transposition and amplification of oncogene-related sequences in human neuroblastomas. Cell 1983;35:359–67.
5. Liu X, Mazanek P, Dam V, et al. Deregulated Wnt/β-catenin program in high-risk neuroblastomas without MYCN amplification. Oncogene 2008;27:1478–88.
6. Adhikary S, Eilers M. Transcriptional regulation and transformation by Myc proteins. Nat Rev Mol Cell Biol 2005;6:635–45.
7. Patel JH, Loboda AP, Showe MK, Showe LC, McMahon SB. Analysis of genomic targets reveals complex functions of MYC. Nat Rev Cancer 2004;4:562–8.
8. O'Connell BC, Cheung AF, Simkevich CP, et al. A large scale genetic analysis of c-Myc-regulated gene expression patterns. J Biol Chem 2003;278:12563–73.
9. Bello-Fernandez C, Packham G, Cleveland JL. The

ornithine decarboxylase gene is a transcriptional target of c-Myc. Proc Natl Acad Sci U S A 1993;90:7804–8.
10. Auvinen M, Paasinen A, Andersson LC, Holtta E. Ornithine decarboxylase activity is critical for cell transformation. Nature 1992;360:355–8.
11. Pegg AE. Polyamine metabolism and its importance in neoplastic growth and a target for chemotherapy. Cancer Res 1988;48:759–74.
12. Bettuzzi S, Davalli P, Astancolle S, et al. Coordinate changes of polyamine metabolism regulatory proteins during the cell cycle of normal human dermal fibroblasts. FEBS Lett 1999;446:18–22.
13. Shirahata A, Pegg AE. Regulation of *S*-adenosylmethionine decarboxylase activity in rat liver and prostate. J Biol Chem 1985;260:9583–8.
14. Gerner EW, Meyskens FL, Jr. Polyamines and cancer: old molecules, new understanding. Nat Rev Cancer 2004;4:781–92.
15. Nilsson JA, Keller UB, Baudino TA, et al. Targeting ornithine decarboxylase in Myc-induced lymphomagenesis prevents tumor formation. Cancer Cell 2005;7:433–44.
16. George RE, Li S, Medeiros-Nancarrow C, et al. High-risk neuroblastoma treated with tandem autologous peripheral-blood stem cell-supported transplantation: long-term survival update. J Clin Oncol 2006;24:2891–6.
17. Maris JM, Hogarty MD, Bagatell R, Cohn SL. Neuroblastoma. Lancet 2007;369:2106–20.
18. Wang Q, Diskin S, Rappaport E, et al. Integrative genomics identifies distinct molecular classes of neuroblastoma and demonstrates that multiple genes are targeted by regional alterations in DNA copy number. Cancer Res 2006;66:6050–62.
19. Manduchi E, Grant GR, McKenzie SE, Overton GC, Surrey S, Stoeckert CJ, Jr. Generation of patterns from gene expression data by assigning confidence to differentially expressed genes. Bioinformatics 2000;16:685–98.
20. Greshock J, Naylor TL, Margolin A, et al. 1-Mb resolution array-based comparative genomic hybridization using a BAC clone set optimized for cancer gene analysis. Genome Res 2004;14:179–87.
21. Mosse YP, Diskin SJ, Wasserman N, et al. Neuroblastomas have distinct genomic DNA profiles that predict clinical phenotype and regional gene expression. Genes Chromosomes Cancer 2007;46:936–49.
22. Haber M, Smith J, Bordow SB, et al. Association of high-level MRP1 expression with poor clinical outcome in a large prospective study of primary neuroblastoma. J Clin Oncol 2006;24:1546–53.
23. Thompson PM, Maris JM, Hogarty MD, et al. Homozygous deletion of CDKN2A (p16INK4a/p14ARF) but not within 1p36 or at other tumor suppressor loci in neuroblastoma. Cancer Res 2001;61:679–86.
24. Tajiri T, Liu X, Thompson PM, et al. Expression of a MYCN-interacting isoform of the tumor suppressor BIN1 is reduced in neuroblastomas with unfavorable biological features. Clin Cancer Res 2003;9:3345–55.
25. Xing JZ, Zhu L, Jackson JA, et al. Dynamic monitoring of cytotoxicity on microelectronic sensors. Chem Res Toxicol 2005;18:154–61.
26. Burkhart CA, Cheng AJ, Madafiglio J, et al. Effects of MYCN antisense oligonucleotide administration on tumorigenesis in a murine model of neuroblastoma. J Natl Cancer Inst 2003;95:1394–403.
27. Hansford LM, Thomas WD, Keating JM, et al. Mechanisms of embryonal tumor initiation: distinct roles for MycN expression and MYCN amplification. Proc Natl Acad Sci U S A 2004;101:12664–9.
28. Weiss WA, Aldape K, Bishop JM. Targeted expression of NMYC causes neuroblastoma in transgenic mice. EMBO J 1997;16:2985–95.
29. Koza RA, Megosh LC, Palmieri M, O'Brien TG. Constitutively elevated levels of ornithine and polyamines in mouse epidermal papillomas. Carcinogenesis 1991;12:1619–25.
30. Cohn SL, London WB, Huang D, et al. MYCN expression is not prognostic of adverse outcome in advanced-stage neuroblastoma with nonamplified MYCN. J Clin Oncol 2000;18:3604–13.
31. Schipper RG, Romain N, Otten AA, Tan J, Lange WP, Verhofstad AA. Immunocytochemical detection of ornithine decarboxylase. J Histochem Cytochem 1999;47:1395–404.
32. Kaplan EL, Meier P. Nonparametric estimation from incomplete observations. J Am Stat Assoc 1958;53:457–81.
33. Peto R, Peto J. Asymptotically efficient rank invariant test procedures. J R Stat Soc A 1972;34:187–220.
34. London WB, Castleberry RP, Matthay KK, et al. Evidence for an age cutoff greater than 365 days for neuroblastoma risk group stratification in the Children's Oncology Group. J Clin Oncol 2005;23:6459–65.
35. Weber A, Imisch P, Bergmann E, Christiansen H. Coamplification of DDX1 correlates with an improved survival probability in children with MYCN-amplified human neuroblastoma. J Clin Oncol 2004;22:2681–90.
36. Cohn SL, Salwen H, Quasney MW, et al. Prolonged N-myc protein half-life in a neuroblastoma cell line lacking N-myc amplification. Oncogene 1990;5:1821–7.
37. Wallick CJ, Gamper I, Thorne M, et al. Key role for p27Kip1, retinoblastoma protein Rb, and MYCN in polyamine inhibitor-induced $G_1$ cell cycle arrest in MYCN-amplified human neuroblastoma cells. Oncogene 2005;24:5606–18.
38. Hackett CS, Hodgson JG, Law ME, et al. Genome-wide array CGH analysis of murine neuroblastoma reveals distinct genomic aberrations which parallel those in human tumors. Cancer Res 2003;63:5266–73.
39. Mosse YP, Greshock J, Margolin A, et al. High-resolution detection and mapping of genomic DNA alterations in neuroblastoma. Genes Chromosomes Cancer 2005;43:390–403.
40. Chesler L, Goldenberg DD, Seales IT, et al. Malignant progression and blockade of angiogenesis in a murine transgenic model of neuroblastoma. Cancer Res 2007;67:9435–42.
41. Wartiovaara K, Barnabe-Heider F, Miller FD, Kaplan DR. N-myc promotes survival and induces S-phase entry of postmitotic sympathetic neurons. J Neurosci 2002;22:815–24.
42. Lan L, Trempus C, Gilmour SK. Inhibition of ornithine decarboxylase (ODC) decreases tumor vascularization and reverses spontaneous tumors in ODC/Ras transgenic mice. Cancer Res 2000;60:5696–703.
43. Matthay KK, Villablanca JG, Seeger RC, et al. Treatment of high-risk neuroblastoma with intensive chemotherapy, radiotherapy, autologous bone marrow transplantation, and 13-*cis*-retinoic acid. Children's Cancer Group. N Engl J Med 1999;341:1165–73.
44. Keller UB, Old JB, Dorsey FC, et al. Myc targets Cks1 to provoke the suppression of p27(Kip1), proliferation and lymphomagenesis. EMBO J 2007;26:2562–74.
45. Basuroy UK, Gerner EW. Emerging concepts in targeting the polyamine metabolic pathway in epithelial cancer chemoprevention and chemotherapy. J Biochem (Tokyo) 2006;139:27–33.
46. Casero RA, Jr., Marton LJ. Targeting polyamine metabolism and function in cancer and other hyperproliferative diseases. Nat Rev Drug Discov 2007;6:373–90.
47. Meyskens FL, Jr., Gerner EW. Development of difluoromethylornithine (DFMO) as a chemoprevention agent. Clin Cancer Res 1999;5:945–51.
48. Varma R, Hector S, Greco WR, et al. Platinum drug effects on the expression of genes in the polyamine pathway: time-course and concentration-effect analysis based on Affymetrix gene expression profiling of A2780 ovarian carcinoma cells. Cancer Chemother Pharmacol 2007;59:711–23.